Construction of CPEB mutants

Point mutations were made with a Chamaleon mutagenesis kit (Stratagene). The selection primer was located in plasmid pMyc–CPEB[5], 5′-CCTCGAGGGGCGGGCCCGTACCC-AATTCGCCC-3′, and changed a *Kpn*I site to a *Srf*I site. This primer was used in conjunction with the following mutation primers to create new clones: serines 174 and 180 to alanine (CPEB-AA), 5′-GCTCTCGATTGGACGCCCGGTCTATTTTGGATGCTC-GCTCC-3′; and serines 174 and 180 to aspartic acid (CPEB-DD), 5′-GCTCTCGATTG-GACGATCGCTCTATTTTGGATGATCGCTCC-3′. The His-tagged form of the mutant CPEBs was obtained by subcloning the *Nco*I–*Bam*HI fragment of CPEB-AA and CPEB-DD into the *Nco*I and *Bam*HI sites of pHis–CPEB[6].

Received 15 November 1999; accepted 24 January 2000.

1. Hake, L. E. & Richter, J. D. Translational regulation of maternal mRNA. *Biochim. Biophys. Acta* **1332,** M31–M38 (1997).
2. Fox, C. A., Sheets, M. D., Wahle, E. & Wickens, M. P. Polyadenylation of maternal mRNA during oocyte maturation: poly(A) addition *in vitro* requires a regulated RNA binding activity and a poly(A) polymerase. *EMBO J.* **11,** 5021–5032 (1992).
3. McGrew, L. L., Dworkin-Rastl, E., Dworkin, M. B. & Richter, J. D. Poly(A) elongation during *Xenopus* oocyte maturation is required for translational recruitment and is mediated by a short sequence element. *Gene Dev.* **3,** 803–815 (1989).
4. McGrew, L. L. & Richter, J. D. Translational control by cytoplasmic polyadenylation during *Xenopus* oocyte maturation: characterization of *cis* and *trans* elements and regulation by cyclin/MPF. *EMBO J.* **9,** 3743–3751 (1990).
5. Hake, L. E. & Richter, J. D. CPEB is a specificity factor that mediates cytoplasmic polyadenylation during *Xenopus* oocyte maturation. *Cell* **79,** 617–627 (1994).
6. Stebbins-Boaz, B., Hake, L. E. & Richter, J. D. CPEB controls the cytoplasmic polyadenylation of cyclin, Cdk2 and c-*mos* mRNAs and is necessary for oocyte maturation in *Xenopus*. *EMBO J.* **15,** 2582–2592 (1996).
7. Paris, J., Swenson, K., Piwnica-Worms, H. & Richter, J. D. Maturation-specific polyadenylation: *in vitro* activation by p34^{cdc2} and phosphorylation of a 58-kD CPE-binding protein. *Genes Dev.* **5,** 1697–1708 (1991).
8. De Moor, C. H. & Richter, J. D. The *mos* pathway regulates cytoplasmic polyadenylation in *Xenopus* oocytes. *Mol. Cell. Biol.* **17,** 6419–6426 (1997).
9. Ballantyne, S., Daniel, D. L. Jr & Wickens, M. A dependent pathway of cytoplasmic polyadenylation reactions linked to cell cycle control by c-*mos* and CDK1 activation. *Mol. Biol. Cell* **8,** 1633–1648 (1997).
10. Katsu, Y., Minshall, N., Nagahama, Y. & Standart, N. Ca^{2+} is required for phosphorylation of clam p82/CPEB *in vitro*: implications for dual and independent roles of MAP and Cdc2 kinases. *Dev. Biol.* **209,** 186–199 (1999).
11. De Moor, C. H. & Richter, J. D. Cytoplasmic polyadenylation elements mediate masking and unmasking of cyclin B1 mRNA. *EMBO J.* **18,** 2294–2303 (1999).
12. Andresson, T. & Ruderman, J. V. The kinase Eg2 is a component of the *Xenopus* oocyte progesterone-activated signaling pathway. *EMBO J.* **17,** 5627–5637 (1998).
13. Glover, D. M., Leibowitz, M. H., McLean, D. A. & Parry, H. Mutations in aurora prevent centrosome separation leading to the formation of monopolar spindles. *Cell* **81,** 95–105 (1995).
14. Francisco, L., Wang, W. & Chan, C. S. Type 1 protein phosphatase acts in opposition to Ipl-1 protein kinase in regulating yeast chromosome segregation. *Mol. Cell Biol.* **14,** 4731–4740 (1994).
15. Bischoff, J. R. *et al.* A homologue of *Drosophila aurora* kinase is oncogenic and amplified in human colorectal cancers. *EMBO J.* **17,** 3052–3065 (1998).
16. Zhou, H. *et al.* Tumour amplified kinase STK15/BTAK induces centrosome amplification, aneuploidy and transformation. *Nature Genet.* **20,** 189–193 (1998).
17. Sen, S., Zhou, H. & White, R. A. A putative serine/threonine kinase encoding gene BTAK on chromosome 20q13 is amplified and overexpressed in human breast cancer cell lines. *Oncogene* **14,** 2195–2200 (1997).
18. Tatsuka, M. *et al.* Multinuclearity and increased ploidy caused by overexpression of the aurora- and Ipl1-like midbody-associated protein mitotic kinase in human cancer cells. *Cancer Res.* **58,** 4811–4816 (1998).
19. Giet, R., Uzbekov, R., Cubizolles, F., Le Guellec, K. & Prigent, C. The *Xenopus laevis* Aurora-related protein kinase pEg2 associates with and phosphorylates the kinesin-related protein XIEg5. *J. Biol. Chem.* **274,** 15005–15013 (1999).
20. Hake, L. E., Mendez, R. & Richter, J. D. Specificity of RNA binding by CPEB: Requirement for RNA recognition motifs and a novel zinc finger. *Mol. Cell. Biol.* **18,** 685–693 (1998).
21. Bilger, A., Fox, C. A., Wahle, E. & Wickens, M. Nuclear polyadenylation factors recognize cytoplasmic polyadenylation elements. *Genes Dev.* **8,** 1106–1116 (1994).
22. Dickson, K. S., Bilger, A., Ballantyne, S. & Wickens, M.P. The cleavage and polyadenylation specificity factor in *Xenopus laevis* oocytes is a cytoplasmic factor involved in regulated polyadenylation. *Mol. Cell. Biol.* **19,** 5707–5717 (1999).
23. Stebbins-Boaz, B., Cao, Q., de Moor, C. H., Mendez, R. & Richter, J. D. Maskin is a CPEB associated factor that transiently interacts with eIF-4E. *Mol. Cell* **4,** 1017–1027 (1999).
24. Boyle, W. J., van der Geer, P. & Hunter, T. Phosphopeptide mapping and phosphoamino acid analysis by two-dimensional separation on thin-layer cellulose plates. *Methods Enzymol.* **201,** 110–149 (1991).

Acknowledgements

We thank E. J. Luna for her help with the two-dimensional separation of phosphopeptides, J. Leszyk for amino-acid sequencing, and the W. M. Keck Foundation for support of the Protein Chemistry Facility. We also thank M. Fernandez and members of the Richter laboratory for discussions and critically reading the manuscript. R.M. was supported by a Leukemia Society of America Special Fellow Award and L.E.L. was supported by a National Science Foundation Predoctoral Fellowship. This work was supported by grants from the NIH (to J.V.R. and J.D.R.).

Correspondence and requests for materials should be addressed to J.D.R. (e-mail: joel.richter@umassmed.edu).

The structure of malaria pigment β-haematin

Silvina Pagola*, Peter W. Stephens*, D. Scott Bohle†, Andrew D. Kosar† & Sara K. Madsen†‡

* *Department of Physics & Astronomy, State University of New York, Stony Brook, New York 11794-3800, USA*
† *Department of Chemistry, University of Wyoming, Laramie, Wyoming 82071-3838, USA*
‡ *Present address: Department of Biologic and Materials Sciences, University of Michigan, Ann Arbor, Minnesota 48109, USA*

Despite the worldwide public health impact of malaria, neither the mechanism by which the *Plasmodium* parasite detoxifies and sequesters haem, nor the action of current antimalarial drugs is well understood. The haem groups released from the digestion of the haemoglobin of infected red blood cells are aggregated into an insoluble material called haemozoin or malaria pigment. Synthetic β-haematin (Fe^{III}-protoporphyrin-IX)$_2$ is chemically[1,2], spectroscopically[2,3] and crystallographically[4] identical to haemozoin and is believed to consist of strands of Fe^{III}-porphyrin units, linked into a polymer by propionate oxygen-iron bonds. Here we report the crystal structure of β-haematin determined using simulated annealing techniques to analyse powder diffraction data obtained with synchrotron radiation. The molecules are linked into dimers through reciprocal iron–carboxylate bonds to one of the propionic side chains of each porphyrin, and the dimers form chains linked by hydrogen bonds in the crystal. This result has implications for understanding the action of current antimalarial drugs and possibly for the design of new therapeutic agents.

Numerous mechanisms have been proposed for the drug action of the quinoline-based antimalarials such as chloroquine[5], but consensus has only been reached regarding its localization in the digestive vacuole of the trophozoite[6,7], its *in vitro* disruption of haem aggregation or detoxification[8,9], and its association with haemozoin[10]. The structure of haemozoin remains speculative despite the many spectroscopic tools used to characterize it[2–4,11,12]. This aggregated product of haem detoxification is now believed to be a coordination polymer[2–4,8–10,13–16], principally because of the η^1-carboxylate links between the iron and the propionate of an adjacent haem, and because monomeric haematin (Fe^{III}-protoporphyrin-IX

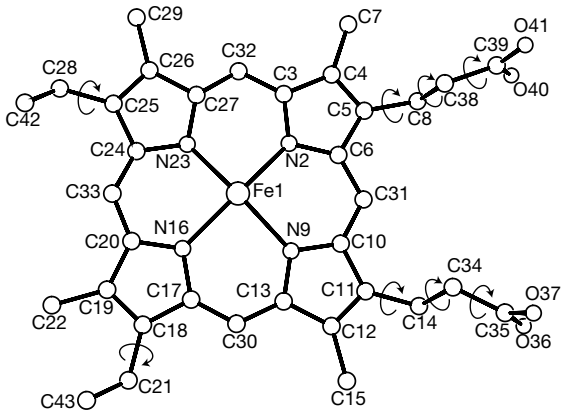

Figure 1 Representation of the Fe^{III}-protoporphyrin-IX molecule used in the structure solution (hydrogen atoms not shown). The arrows indicate torsional degrees of freedom for the vinyl and propionic acid groups. This illlustration corresponds to the molecular conformation obtained in the structure solution.

(OH)) dissolves more readily than β-haematin in aqueous and coordinating solvents.

Here we describe the crystal structure of β-haematin, a well-known synthetic analogue of haemozoin. For this work to be directly relevant to malarial haemozoin, we needed to establish that the crystal structures of these two solids are identical. β-haematin is spectroscopically identical to haemozoin that is isolated from or found in malarial trophozoites[2,3], but this alone is not sufficient proof of solid-state structural identity. Previously, we prepared homogenous single-phase microcrystalline powders of β-haematin from the dehydrohalogenation of haemin[17] and compared their powder X-ray diffraction patterns with those of whole dried parasitized red blood cells[4]. The diffraction patterns are visually identical, implying that they both correspond to the same triclinic unit cell and are isostructural at the atomic level; therefore, to solve the structure of one phase is to solve the structure of both. Two factors favour the use of synthetic β-haematin for the crystallographic analysis: a better signal-to-background ratio in the diffracted intensity, and the observation of sharper diffraction peaks. Neither of these indicates a difference in the atomic structure within each unit cell; therefore, the current results are directly transferable to natural haemozoin.

We collected high-resolution X-ray powder diffraction data at beamline X3B1 of the National Synchrotron Light Source from samples of β-haematin, both in a 1-mm capillary and in a flat-plate sample holder. The powder patterns indexed to a triclinic unit cell, a = 12.196(2) Å, b = 14.684(2) Å, c = 8.040(1) Å, α = 90.22(1)°, β = 96.80(1)°, γ = 97.92(1)°; V = 1416.0(3) Å^3; ρ_{exp} = 1.45(1) g cm^{-3}; Z = 2, which is essentially identical to earlier results[3,4] for other batches of β-haematin. We determined the structure by a simulated annealing algorithm, similar to described methods[18,19]. Briefly, the chemical structure of the Fe^{III}-protoporphyrin-IX unit is known (Fig. 1), implying that the previous estimates of all bond distances and angles were good, although the eight torsion angles per molecule have to be determined. We took an initial estimate of the geometry of the porphyrin group from that of haemin[20]. Solving a crystal structure consists of positioning the molecule(s) within the unit cell and finding the torsion angles that give the best agreement between experimental and calculated powder diffraction profiles. For any candidate structure, we define an agreement factor between the observed ($I_{obs}(2\theta)$) and calculated ($I_{calc}(2\theta)$) powder patterns as

$$S = \frac{\int \mathrm{d}2\theta (I_{obs}(2\theta) - I_{calc}(2\theta))^2}{(\int \mathrm{d}2\theta I_{obs}(2\theta))^2}$$

In practice, it is more efficient to compare the integrated intensities of diffraction lines, but their overlap prevents this from being done unambiguously. We have developed a technique that compares integrated intensities A_{hkl} extracted from the data using the Le Bail algorithm[21] with a set of B_{hkl} calculated for a candidate structure. S can be calculated very efficiently by noting that

$$S = \frac{\int \mathrm{d}2\theta \left(\sum_{hkl} A_{hkl} f_{hkl}(2\theta) - \sum_{hkl} B_{hkl} F_{hkl}(2\theta) \right)^2}{\left(\int \mathrm{d}2\theta \sum_{hkl} A_{hkl} f_{hkl}(2\theta) \right)^2}$$

$$= \frac{\sum_{hkl,h'k'l'} (A_{hkl} - B_{hkl}) F_{hkl,h'k'l'} (A_{h'k'l'} - B_{h'k'l'})}{\left(\sum_{hkl} A_{hkl} \right)^2}$$

where $f_{hkl}(2\theta)$ is the profile of the (hkl) powder peak and the overlap

$$F_{hkl,h'k'l'} = \int d2\theta f_{hkl}(2\theta) f_{h'k'l'}(2\theta)$$

is significant for nearby peaks, and only needs to be computed once. A similar method has been described[18], using the Pawley extraction method and the least-squares correlation matrix for $F_{hkl,h'k'l'}$.

Using the first 150 diffraction peaks ($2\theta < 24.82°$) from the capillary data set, we made numerous simulated annealing runs in both triclinic space groups. In $P\bar{1}$, the 2 molecules in the unit cell are related by inversion symmetry, and so there are 14 parameters (3 coordinates for the centre of the molecule, 3 Euler angles to specify its orientation and 8 torsion angles). All of the structures with $S < 0.02$ in space group $P\bar{1}$ were essentially identical. In each of these cases, one of the carboxylic oxygen atoms was in the range of 1.90–2.49 Å from the iron atom, and the oxygen–oxygen distances of the other propionate groups were 3.25–3.97Å. In every one of these solutions, the molecules were paired into dimers by two reciprocal iron–oxygen bonds as shown in Fig. 2. The annealing schedule often could not reach such a low value of S, but these metastable solutions never showed suitable bonding neighbours for the propionic oxygens. Simulated annealing in $P1$ (2 independent molecules, 25 geometrical parameters) also found a candidate structure equivalent to the $P\bar{1}$ structure described above and never found anything with a lower value of S.

A Rietveld refinement of the structure was performed using GSAS[22] on the flat-plate data set. We kept the geometry of the iron–porphyrin ring as a rigid body in the Rietveld refinement, with the high-spin iron ion located 0.47 Å above the plane of the porphyrin ring. Soft bond distance constraints were included for the refinement of the positions and bond angles of the carbon and oxygen atoms of the vinyl and propionic groups. The best refinement obtained has R_{wp} = 6.37%, R_I = 3.0% and χ^2 = 4.2. Correspondent values in the Le Bail fit were R_{wp} = 4.13% and χ^2 = 1.9. Observed and

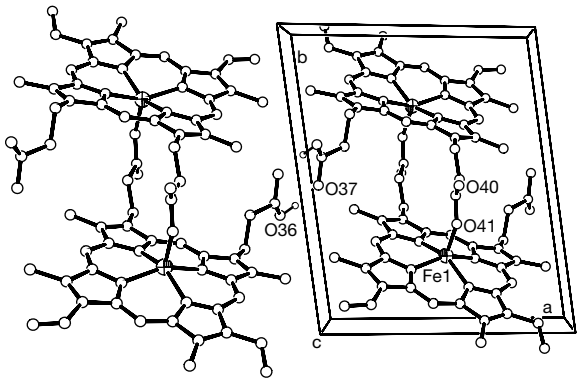

Figure 2 Two unit cells of the crystal structure of β-haematin, viewed along the [001] direction. Formation of dimers occurs through Fe1–O41 bonds, whereas dimers are linked by hydrogen bonds through O36 and O37. All other hydrogens are omitted for clarity.

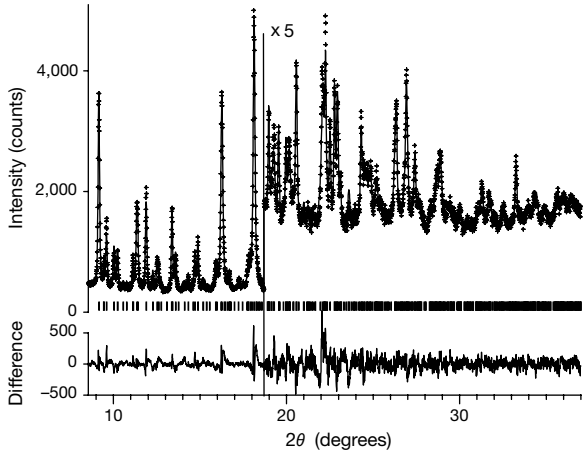

Figure 3 Observed (crosses) and calculated (solid line) X-ray powder diffraction patterns of β-haematin, using X-rays of wavelength 1.16192 Å. The lower trace shows the difference curve.

calculated diffraction patterns are shown in Fig. 3. Given the limitations of the powder diffraction technique on this sample and the size of the molecule (43 non-hydrogen atoms), the atomic coordinates are not as accurately determined as from a typical single-crystal experiment; however, the overall result of the molecular bonding geometry is unequivocally established by this work.

After the Rietveld refinement, there was not significant structure in the Fourier difference map, which ranged between −0.095 and +0.086 e^{-} Å^{-3}. As an independent test of the correctness of the connection topology of the molecules, we ran Fourier difference calculations starting with the atomic positions of only the iron–porphyrin ring. The oxygen bonded to the iron and the two carbons of the propionic side chain are immediately visible. This precludes the possibility that the *S* factor in the structure solution stage is insufficiently sensitive to the propionic chain's positions which might lead to solutions in which these fragments are incorrectly located.

The refined crystal structure is shown in Figs 2 and 4. The inversion symmetry creates the dimer pair in the unit cell, and these in turn stack in the lattice to give parallel iron porphyrin units along the [001] direction. Critical metric parameters include the Fe1–O41 bond distance, which converged to a value 1.886(2) Å. Refinements were satisfactory for O36-H-O37 hydrogen bonds, in the range of 2.8 Å, which is in agreement with crystallographically characterized carboxylic acid dimers. The Fe–O bond length is not significantly different from those found for high-spin ferric complexes of synthetic porphyrins, for example 1.898(4) Å (acetate) and 1.847(2) Å (phenoxide)[23]. The refined atomic coordinates and selected bond distances and angles are given in the Supplementary Information.

This structure is consistent with all of the known spectroscopic[1–3] and magnetic[3,11] properties of β-haematin. To our knowledge[24], there has been no observation of a porphyrin dimer in which the metal atoms are reciprocally esterified by the side chains. A similar idea was first suggested[25] in 1949, but in that model, dimerization was proposed to be by ion pairing of a cationic six-coordinate iron to anionic propionates, which has never been experimentally confirmed.

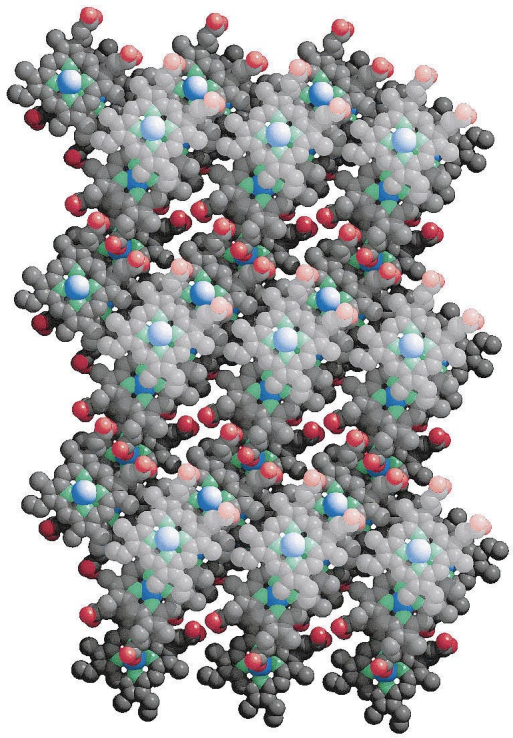

Figure 4 Packing diagram of the crystal structure of β-haematin. The [131] face, which is roughly parallel to the porphyrin rings, is in the plane of the paper. Lighter shaded atoms (C, grey; O, red; N, green; Fe, blue; H, not shown) are nearer the viewer. The chains of hydrogen-bonded dimers extend from left to right.

Comparing the solubilities of haematin and β-haematin, in sufficiently alkaline solutions β-haematin will dissolve, presumably by solvation of the free carboxylate groups and rupture of the iron–carboxylate bonds. This will be true for either the dimer described here or the previously proposed polymer. On the basis of our structure, the difference in solubilities in coordinating solvents such as pyridine and dimethyl sulphoxide might be due to a chelate effect in which the kinetics of iron–carboxylate bond substitution are retarded owing to the dimeric nature of β-haematin; the rate of the back reaction following solvolysis of one Fe–OC(O) bond to the dimer will compete with the solvolysis of the second Fe–OC(O) bond to give to completely separate monomers. In the case of a polymer, each solvolysis reaction will lead to liberation of a haem. However, any discussion of solubilization of these species requires full consideration of the inhomogenous kinetics of the crystal/solution interface, and these will be markedly influenced by crystallite morphology, size and the solute–solution interaction. Consequently, the observed solubility characteristics alone are insufficient evidence for the polymeric structure.

In vitro experiments have established that the quinoline antimalarial drugs are associated with the crystallization of haemazoin[10]. This suggests that their therapeutic effect occurs by interference with the formation of that solid phase. Proposed mechanisms for such a drug action can be grouped into three categories: (1) direct binding of the drug to haem monomers or dimers in solution[13], which interferes with the crystallization of haemozoin; (2) enzymatic inhibition of a protein that catalyses haemazoin crystallization[8]; and (3) chemiabsorption of the drug onto crystallized haemazoin, leading to inhibition of further haem aggregation[26].

Some models in the first category[10,13] have proposed a haem–drug complex capping the extension of a presumed haematin polymer. As we have established that haemazoin is not a coordination polymer so that the growth of a chain cannot be stopped at a single site, these models must be re-examined. This is not merely a semantic difference, that is to substitute crystallization for polymerization. Any such model now has to explain how a ~1 mM intravacuolar[27] concentration of chloroquine could act catalytically to maintain a sufficient (~0.4 M) concentration of free haematin[10] to disrupt the *Plasmodium* trophozoites and display the known therapeutic action.

The second category of models suggests that a protein mediates haem aggregation into haemozoin, and that the action of quinoline drugs is to inhibit this supposed haem polymerase[8]. The fact that quinoline inhibits the growth of haemozoin *in vitro* argues against this hypothesis, although the *in vitro* growth of haemozoin at physiological pH and temperature has not been unequivocally shown. Unfortunately, the isolation of proteinaceous fractions from *Plasmodium* trophozoites with unambiguous activity to form haemozoin has been controversial, and considerable uncertainty lingers over the role of enzyme in the aggregation/detoxification process[9,14,15].

Finally, the haematin–quinoline complex may not be covalently bonded to haemozoin[10], and an evaluation of all of these mechanisms has led to the proposal of a general and as yet undetermined surface–drug interaction as the origin of quinoline's drug action[26]. Both natural and synthetic malaria pigment crystallize as long thin needles[28], whose approximate dimensions are 1.0 ± 0.1 μm, 0.6 ± 0.1 μm and 0.2 ± 0.1 μm, as isolated from mature trophozoites. These remarkably uniformly sized and shaped crystals have estimated volumes and surface areas of 0.1 μm^3 and 2 μm^2

respectively. Together, these crystals feature a pair of relatively small, fast-growing faces which correspond to ~5% of the total crystal surface area. The hypothesis that antimalarial drug action of quinoline arises from surface absorption on the actively growing faces of malaria pigment crystallites is entirely consistent with the following estimate of ~8% surface area coverage for the final crystallites. (The experimentally determined density for malaria pigment, $\rho = 1.45(1)$ g cm^{-3} from the structure and unit cell, indicates that there are 0.3 fmol of haem per crystal, and thus in a typical 80-fl red blood cell with a haemoglobin concentration of 20 mM there is enough haem to make about 10 of the final malaria pigment crystals. Absorption coverage is based on estimates of the intravacuolar chloroquine concentration of ~1 mM and chloroquine's predicted Connolly surface coverage of ~300 Å^2.) Clearly, for crystallites formed and growing in the young trophozoites, there will be more than sufficient chloroquine to ensure complete surface coverage, although we note that we are not aware of any experimental description of either the number or morphology of the crystallites isolated from young trophozoites. The hypothesis of a surface adsorption process limiting new haem uptake is therefore plausible, and this work provides impetus to further determine the surface structure and chemistry of malaria pigment.

Haemoglobin catabolism and β-haematin formation in the *Plasmodum* trophozoite is a highly organized process designed not just to efficiently deliver amino acids for *de novo* protein synthesis, but also to avoid the build-up and adventitious release of free haem. The organization of digestive vacuole haemoglobin peptidases is well understood[16,29,30]. In contrast, issues regarding iron oxidation and haemozoin nucleation and growth remain poorly explained, and these must be considered as potential drug targets. Although there is evidence that quinoline surface adhesion is present, and contributes to the remarkable concentration of drug within the digestive vacuole of *Plasmodium*, there may be other interactions that also contribute to their drug action. Detailed information concerning all levels of intravacuolar haem processing is required if the biochemistry of haem detoxification is to be understood at a more meaningful level. The unexpected observation of haem dimers in the solid malaria pigment is a fundamental ingredient of any such description. □

Received 2 November 1999; accepted 7 January 2000.

1. Fitch, C. D. & Kanjananggulpan, P. The state of ferriprotoporphyrin IX in malaria pigment. *J. Biol. Chem.* **262,** 15552–15555 (1987).
2. Slater, A. F. G. *et al.* An iron–carboxylate bond links the heme units of malaria pigment. *Proc. Natl Acad. Sci. USA* **88,** 325–329 (1991).
3. Bohle, D. S. *et al.* Structural and spectroscopic studies of β-hematin (the heme coordination polymer in malaria pigment. *Am. Chem. Soc. Symp. Ser.* **572,** 497–515 (1994).
4. Bohle, D. S., Dinnebier, R. E., Madsen, S. K. & Stephens, P. W. Characterization of the products of the heme detoxification pathway in malarial late trophozoites by X-ray diffraction. *J. Biol. Chem.* **272,** 713–716 (1997).
5. Olliaro, P. L. & Goldberg, D. E. The plasmodium digestive vacuole- metabolic headquarters and choice drug target. *Parasitol. Today* **11,** 294–297 (1995).
6. Yayon, A., Cabantchik, I. & Ginsburg, H. Susceptibility of human malaria parasites to chloroquine is pH dependent. *Proc. Natl Acad. Sci. USA* **82,** 2784–2788 (1985).
7. Homewood, C., Warhurst, D., Peters, W. & Baggaley, V. Lysosomes, pH and the anti-malarial action of chloroquine. *Nature* **235,** 50–52 (1972).
8. Slater, A. F. G. & Cerami, A. Inhibition by chloroquine of a novel haem polymerase enzyme activity in malaria trophozoites. *Nature* **355,** 167–169 (1992).
9. Dorn, A., Stoffel, R., Matile, H., Bubendorf, A. & Ridley, R. G. Malarial haemozoin/β-haematin supports haem polymerization in the absence of protein. *Nature* **374,** 269–271 (1995).
10. Sullivan, D. J., Gluzman, I. Y., Russell, D. G. & Goldberg, D. E. On the molecular mechanism of chloroquine's antimalarial action. *Proc. Natl Acad. Sci. USA* **93,** 11865–11870 (1996).
11. Bohle, D. S., Debrunner, P., Jordan, P. A., Madsen, S. K. & Schulz, C. E. Aggregated heme detoxification byproducts in malarial trophozoites: β-hematin and malaria pigment have a single S = 5/2 iron environment in the bulk phase as determined by EPR and magnetic Mössbauer spectroscopy. *J. Am. Chem. Soc.* **120,** 8255–8256 (1998).
12. Adams, P. A., Berman, P. A. M., Egan, T. J., Marsh, P. J. & Silver, J. The iron environment in heme and heme-antimalarial complexes of pharmacological interest. *J. Inorg. Biochem.* **63,** 69–77 (1996).
13. Dorn, A. *et al.* An assessment of drug–haematin binding as a mechanism for inhibition of haematin polymerisation by quinoline antimalarials. *Biochem. Pharmacol.* **55,** 727–736 (1998).
14. Bendrat, K., Berger, B. J. & Cerami, A. Haem polymerization in malaria. *Nature* **378,** 138 (1995).
15. Ridley, R. G., Dorn, A., Matile, H. & Kansy, M. Haem polymerization in malaria. *Nature* **378,** 138–139 (1995).
16. Francis, S. E., Sullivan, D. J. & Goldberg, D. E. Hemoglobin metabolism in the malaria parasite *Plasmodium falciparum*. *Annu. Rev. Microbiol.* **51,** 97–123 (1997).
17. Bohle, D. S. & Helms, J. B. Synthesis of beta-hematin by dehydrohalogenation of hemin. *Biochem. Biophys. Res. Commun.* **193,** 504–508 (1993).
18. David, W. I. F., Shankland, K. & Shankland, N. Routine determination of molecular crystal structures from powder diffraction data. *Chem. Commun.* 931–932 (1998).
19. Andreev, Y. G. & Bruce, P. G. Solving crystal structures of molecular solids without single crystals: a simulated annealing approach. *J. Chem. Soc. Dalton Trans.* 4071–4080 (1998).
20. Koenig, D. F. The structure of α-chlorohemin. *Acta Crystallogr.* **18,** 663–673 (1965).
21. LeBail, A., Duroy, H. & Fourquest, J. L. *Ab initio* structure determination of $LiSbWO_6$ by X-ray-powder diffraction. *Mater. Res. Bull.* **23,** 447–452 (1988).
22. Larson, A. C. & Von Dreele, R. B. *GSAS General Structure Analysis System* (Los Alamos Laboratory Report No. LA-UR-86-748, Los Alamos, 1987).
23. Bominaar, E. L. *et al.* Structural, Mossbauer, and EPR investigations on two oxidation states of a five-coordinate, high spin synthetic heme. Quantitative interpretation of zero-field parameters and large quadrupole splitting. *Inorg. Chem.* **31,** 1845–1854 (1992).
24. Scheidt, W. R. & Lee, Y. J. Recent advances in the stereochemistry of metallotetrapyrroles. *Struct. Bond.* **64,** 1–70 (1987).
25. Lemberg, R. & Legge, J. W. *Haematin Compounds and Bile Pigments* (Interscience, New York, 1949).
26. Sullivan, D. J., Matile, H., Ridley, R. G. & Goldberg, D. E. A common mechanism for blockade of heme polymerization by antimalarial quinolines. *J. Biol. Chem.* **273,** 31103–31107 (1998).
27. Slater, A. F. G. Chloroquine-mechanism of drug-action and resistance in *Plasmodium falciparum*. *Pharm. Ther.* **57,** 203–235 (1993).
28. Egan, T. J., Hempelmann, E. & Mavuso, W. W. Characterisation of synthetic beta-haematin and effects of the antimalarial drugs quinidine, halofantrine, desbutylhalofantrine and mefloquine on its formation. *J. Inorg. Biochem.* **73,** 101–107 (1999).
29. Gluzman, I. Y. *et al.* Order and specificity of the *Plasmodium falciparum* hemoglobin degradation pathway. *J. Clin. Invest.* **93,** 1602–1608 (1994).
30. Francis, S. E., Gluzman, I. Y., Oksman, A., Banerjee, D. & Goldberg, D. E. Characterization of native falcipain, an enzyme involved in *Plasmodium falciparum* hemoglobin degradation. *Mol. Biochem. Parasitol.* **83,** 189–200 (1996).

Supplementary information is available from *Nature*'s World-Wide Web site (http://www.nature.com) or as paper copy from the London editorial office of *Nature*.

Acknowledgements

The National Synchrotron Light Source, Brookhaven National Laboratory, is supported by the US Department of Energy, Division of Chemical Sciences and Division of Materials Sciences. D.S.B. acknowledges financial support from Dreyfus Foundation and the United Nations Development Programs/World Bank/World Health Organisation Special Programme for Research and Training in Tropical Diseases. The SUNY X3 beamline at the National Synchrotron Light Source is supported by the Division of Basic Energy Sciences of the US Department of Energy.

Correspondence and requests for materials should be addressed to P.W.S. (e-mail: peter.stephens@sunysb.edu).